machines

MDPI

Article

Modeling and Application of an SMA-Actuated Lightweight Human-Inspired Gripper for Aerial Manipulation

Vicente Perez-Sanchez, Francisco Javier Garcia-Rubiales, Saeed Rafee Nekoo, Begoña Arrue * and Anibal Ollero

GRVC Robotics Laboratory, University of Seville, Avenida de los Descubrimientos S/N, 41092 Seville, Spain; vpsanchez@us.es (V.P.-S.); javiergaru92@gmail.com (F.J.G.-R.); saerafee@yahoo.com (S.R.N.); aollero@us.es (A.O.)
* Correspondence: barrue@us.es

Abstract: The increasing usage of multi-rotor aerial platforms and the reliability of flights enabled researchers to add equipment and devices to them for application. The addition of lightweight manipulators, grippers, and mechanisms to fulfill specific tasks has been reported frequently recently. This work pushes the idea one step ahead and uses an Artificial Human Hand (AHH) in an uncrewed aerial vehicle for aerial manipulation, device delivery, and co-operation with human workers. This application requires an effective end-effector capable of grasping and holding objects of different shapes. The AHH is a lightweight custom-made human-inspired design actuated using Shape Memory Alloy (SMA) materials. The SMA actuators offer significantly high forces with respect to their light weights though the control of these new actuators is a challenge that has been successfully demonstrated in this paper. The control of the SMA actuators could be achieved via heat exchange on the actuator, indirectly carried out by changing the current. The benefit of using this new actuator is removing the motors and mechanical mechanisms and simplifying the design. A soft cover is developed for the AHH to add friction and make it closer to a human hand. The modeling of the structured actuators on the system through tendons is presented, and a series of experiments for handling and manipulating different objects have been conducted. The objects were chosen with different weights and shapes to show the effectiveness of the design. An analysis of a generated torque of the manipulator for different cylindrical objects has been carried out. An analysis and comparison for grasping a series of items, pressure and temperature analysis, and the weight-to-volume ratio have been presented.

Keywords: aerial robotics; aerial manipulation; artificial human hand; sma actuators; human inspired gripper

Citation: Perez-Sanchez, V.; Garcia-Rubiales, F.J.; Nekoo, S.R.; Arrue, B.; Ollero, A. Modeling and Application of an SMA-Actuated Lightweight Human-Inspired Gripper for Aerial Manipulation. *Machines* **2023**, *11*, 859. https://doi.org/10.3390/machines11090859

Academic Editors: Fernando Gómez-Bravo and Zheng Chen

Received: 27 June 2023
Revised: 15 August 2023
Accepted: 24 August 2023
Published: 27 August 2023

1. Introduction

The bioinspired design has been an influential approach in engineering, taking inspiration from nature to create innovative and efficient solutions to various challenges. Unmanned Aerial Vehicles (UAVs) are no exception, as researchers and engineers are turning to biological systems to develop bioinspired elements to enhance the flight capabilities of these aerial platforms. By emulating the structures and behaviors found in nature, bioinspired UAVs aim to achieve improved maneuverability, efficiency, and adaptability [1–3].

An application of aerial manipulation is the collaboration with human workers, which needs an effective gripper with a safe distance from the multirotor platform. The propellers of the multirotor drone must be far enough from a human worker to avoid any danger. "AERIAL COgnitive integrated multi-task Robotic system with Extended operation range and safety" or the so-called AERIAL-CORE project, aims to investigate this issue within the EU Horizon 2020 framework (https://cordis.europa.eu/project/id/871479, accessed on 23 August 2023). This research presents one of the designed platforms for this project to hand over devices and tools to human workers in high-altitude powerlines. The installation

and manipulation of different devices on powerlines, such as bird diverters, were exercised [4,5], though using human-inspired grippers has rarely been reported. The proposed Artificial Human Hand (AHH) is designed to grasp objects of different shapes and weights for this task. Figure 1 contextualizes this work. The developed gripper aims for safer co-operation with humans at the same time that it is able to transport the tools and objects needed to work in the powerline.

Figure 1. The developed human-inspired manipulator interacting with a human.

The usage of Shape Memory Alloy (SMA) materials is crucial since it reduces the weight of the gripper significantly [6–8]. The application of SMAs in robotics is increasing in various fields, such as medical robotics [9], soft systems [10], lightweight human arm and hand [11], wearable assistive robots [12], etc. Yang et al. presented a robotic arm with a hand, actuated using coil polymer and SMA materials to replicate a human arm [11]. An antagonistic system design was used to represent the motion of the muscles in human arms and system modeling and control design for thermal and position control. Jeong et al. used wearable shape memory alloys to play the role of artificial muscles to assist humans [12]. Similarly, the use of SMA actuators is motivated by its lightweight characteristics, strong force production, and system reliability in the AHH design in this work. The control of the SMA is achieved by increasing or decreasing the temperature of the actuator using a variable current in the system. The flexibility of the SMA actuators allows the device to change its shape while applying force, which provides soft actuation. Soft and shape-changing actuation is ideal for bioinspired and soft robotics.

One prominent example of a bioinspired element in UAV designs is the biomimetic wing and tail structures [13–17]. The wings of birds, insects, and bats have evolved over millions of years to enable efficient flights in diverse environments. Engineers can create UAV wings that exhibit enhanced aerodynamic performance by studying and replicating the structural features of these wings, such as their shape, flexibility, and surface textures. This includes improved lift-to-drag ratios, increased maneuverability, and reduced energy consumption during flight [18–20]. For instance, using flexible wing structures inspired by bird wings allows for adaptive wing morphing, enabling UAVs to adjust their wing shape in real time to optimize performance under different flight conditions [21].

Furthermore, researchers have also drawn inspiration from the efficient flight mechanisms of insects, such as bees and dragonflies, to develop bioinspired propulsion systems for UAVs [22,23]. Engineers have developed flapping-wing UAVs, also known as ornithopters, by studying these insects' unique wing-flapping motion and vorticity control mechanisms. These bioinspired propulsion systems offer advantages in terms of maneuverability, agility, and stability, enabling UAVs to navigate complex and cluttered environments with greater ease [24–26]. The integration of bioinspired elements in UAV designs holds immense potential across various applications, including surveillance and reconnaissance, search and rescue operations, environmental monitoring, and package delivery. By incorporating

bioinspired design principles, UAVs can overcome flight efficiency, agility, and maneuverability challenges, thereby expanding their capabilities and improving their overall performance. In conclusion, bioinspired elements are revolutionizing the field of UAV design, offering insights and solutions derived from nature's evolutionary innovations. By emulating biological systems' structures, mechanisms, and behaviors, engineers are pushing the boundaries of UAV capabilities, resulting in more efficient and versatile aerial platforms. The integration of biomimetic wings and flapping-wing propulsion systems demonstrates the potential of bioinspired design in enhancing the flight characteristics of UAVs. As research in this field continues to evolve, bioinspired UAVs hold great promise for various applications, advancing aerial technology toward more effective and sustainable solutions.

Artificial robotic hands are more feasible due to the advancement of technology recently. Three-dimensional printing is one of the key advancements that emerged from the number of prototypes [27–31]. Bao et al. presented a neuromorphic humanoid hand for grasping objects; the key feature in the design was the origami fingers equipped with a pressure sensor to perform the task [27]. Haptic feedback is also employed for the efficient grasping of AHH to exert proper force for holding objects [31]. The loss of tactile sensations was reported as the major challenge in replicating the dexterity of human hands. Zhou et al. presented a 3D-printed human hand equipped with soft sensors to hold and grasp objects [30]. Gesture control of a human hand was studied, which solved the complex problem of controlling an AHH with many joints [29].

Lightweight end-effectors are necessary for maintenance and inspection tasks, devoted to robots to remove human workers from dangerous sites. Most tasks traditionally were performed by human operators, hanged from the power lines, or placed on elevators. The examples are helical bird diverters [5], clip-type diverters [32], or other types [33]. The idea of a human-inspired robotic hand is to replicate the hand of a worker to fulfill the operation as close as possible to the traditional way. The installation requires two hands for complex scenarios. Consequently, the structure of the human hand was proposed, designed, and experimented to move towards replicating the work of conventional operators. The other advantage of a human hand is the fingers; they provide a perfect grasp from multiple points, which inspired this research. The grasping of a variety of shapes is presented.

The technical problem in this investigation is to design and develop an end-effector for aerial manipulation and tool delivery. A part of this application is inspired by the AERIAL-CORE project, which explicitly demands co-working and collaboration with humans.

The main contribution of this work is to design and prototype an artificial human-like hand actuated using SMA components for installation under a multirotor drone for object manipulation and grasping. The application could be tool delivery to human workers in hard-to-reach sites or interaction with high-voltage powerlines, which is dangerous for human workers.

The rest of this paper is structured as follows. Section 2 expresses the manipulator design and prototyping. Section 3 states the dynamic modeling of the AHH and SMA actuators. Section 4 presents the experimental validation of the system. The conclusions are reported in Section 5.

2. Multiple-Fingered Hand Design

2.1. Multiple-Fingered Hand

This section presents the manipulator design focusing on its characteristics and design requirements to reach the presented solution. The construction of a bioinspired hand involves leveraging modern manufacturing techniques and materials to replicate the form and functionality of a human hand. In this case, the palm and phalanges are constructed using polylactic acid (PLA) and are 3D printed, while the joints are made of a flexible thermoplastic polyurethane (TPU) material to facilitate hand opening and closing. The hand is covered with a silicone skin to enhance grip and provide a textured surface. Additionally,

strategically placed holes are incorporated to allow the passage of cables, which actuate the hand and facilitate proper bending.

The hand joints are constructed using a flexible 3D-printed TPU material. TPU's excellent elasticity and durability enable the hand to articulate smoothly and withstand repetitive motions. The flexibility of the TPU joints allows for easy hand opening and closing, mimicking the natural movements of a human hand. The joints are also available in different lengths; the ones closer to the palm are longer, and the ones further away are shorter. This design ensures that the lower phalanges bend first and the fingertips close last. Figure 2 shows the joints' CAD design and the finger's final assembly.

(**a**) Joints CAD design. (**b**) Finger CAD design.

Figure 2. The construction of phalanges with joints. Both images show the difference in the length of the joints to facilitate finger mobility and improve grip when bent.

Using a 3D printer, the palm and phalanges of the bioinspired hand are manufactured with PLA, a biodegradable and easily moldable thermoplastic. This material offers sufficient strength and rigidity to support the structure of the hand while maintaining a lightweight design. By employing 3D-printing technology, intricate details and customized shapes can be achieved, allowing for a more accurate replication of the human hand's anatomy. Figure 3 shows the different parts of the hand.

(**a**) Hand CAD design. (**b**) Finger CAD design.

Figure 3. Sample of the CAD design of the palm and fingers.

Furthermore, the importance of the strategically placed holes in the hand's structure should not be overlooked. These holes serve as the pathways for the cables that actuate the hand's movements. By carefully routing the cables through these holes, the hand can be controlled to perform intricate finger movements, replicating the dexterity of a real hand. Proper cable management ensures smooth and synchronized motions, allowing for precise control over the opening and closing of the hand's grasp. Figure 4 shows the final assembly (palm, fingers, joints, and kevlar threads).

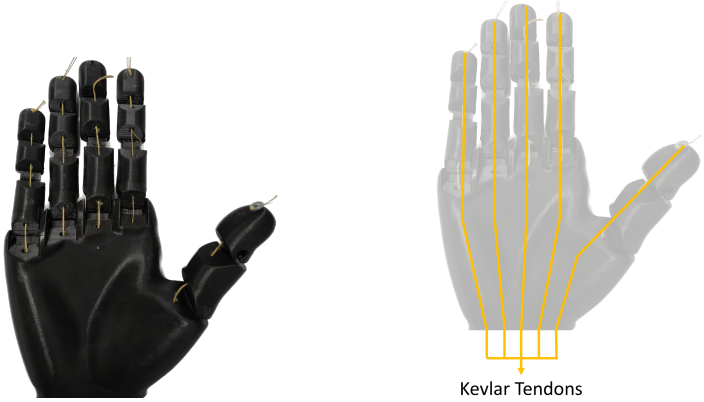

(**a**) Hand final assembly (**b**) Tendons distribution.

Figure 4. This figure shows the final assembly of the hand and the tendons distribution. The figure shows in detail the different holes of the hand for closing and opening, driven by the Kevlar threads. These will be covered with silicone skin.

The silicone skin is applied to the hand to improve grip and enhance its interaction with objects. This material provides a textured surface that enhances friction and grasping capabilities, enabling the hand to securely hold and manipulate objects of various shapes and sizes. Figure 5 shows the silicone skin and palm structure developed to increase replicating the human morphology.

(**a**) Human hand palm structure. (**b**) Developed hand palm structure.

(**c**) Palm skin. (**d**) Back of the hand skin.

Figure 5. The palm structure and skin of the hand. (**a**) shows the palm structure of a human hand. (**b**) shows the palm structure developed. (**c**,**d**) present the silicone-based skin used.

In conclusion, constructing a bioinspired hand involves utilizing 3D-printed PLA for the palm and phalanges, employing flexible TPU for the joints to facilitate movement, applying a silicone skin to enhance grip, and incorporating holes for cable routing to actuate the hand's movements. This combination of materials and design elements brings the bioinspired hand closer to replicating the functionality and versatility of a natural human hand. Figure 6 shows the final construction of the hand, representing the different joints

and the carbon fiber structure used to place the SMA springs that activate the closing and opening of the hand.

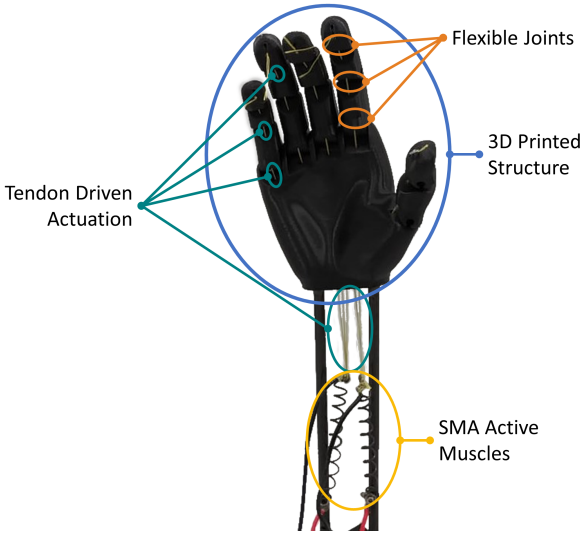

Figure 6. The final hand construction with SMA spring actuators.

2.2. SMA Actuation

SMAs are a special alloy of nickel and titanium (NiTi). They are also called NiTinol. However, this nomenclature is more common in medical devices developed with this alloy. The SMAs are part of the group of smart materials that can change their properties via external stimulations, in the case of the SMA, their Young modulus. The variations of the Young modulus reflect the phase of the alloy's crystalline structure.

Due to the reactivity of the titanium, the manufacturing process of this material is complex. However, their properties justify the cost of manufacturing. The properties that make this alloy distinctive are shape memory and superelasticity. The elasticity of this material is between 10 and 30 times bigger than any other metal. It makes it possible to achieve high deformation, reducing damages to the alloy.

The shape memory effect is the property that transfers the SMAs to an actuator. Depending on the temperature, the material's internal composition varies between martensite and austenite. The SMA at the temperature of the environment is in the martensite phase. Then, the warming material reaches a temperature that changes proportionally between martensite and austenite. In the martensite phase, titanium and nickel exchange positions in the corners of the crystalline structure, reducing the degree of compactness. In the austenite phase, the titanium is positioned in the corners of the cubic structure surrounding the nickel in the center, generating a high degree of compactness. The yield strength of the material reflects this behavior.

The alloy is on the martensite phase at the environmental temperature with a low degree of compactness. Then, by increasing the temperature, the alloy is stable up to the transition temperature. When the alloy reaches the transition temperature, the percentage of the austenite phase increases with the temperature. In the end, the alloy obtains the complete composition of austenite at a defined maximum temperature. If the alloy exceeds this temperature, it starts getting burned, storing a new initial shape. The SMA properties have been widely studied, and more details can be found in Refs. [34–36].

The objective of the actuation is to store an initial shape that generates actuation in the hand's tendons by pulling it. In this case, we propose using SMAs with a spring shape. This geometry makes it possible to perform longitudinal actuation. The memorized geometry is the shape of a compressed spring. Then, the spring is elongated, reaching a detwinned martensite state. At this point, the spring has a permanent deformation. The alloy obtains the austenite state, which increases the Young modulus by increasing the temperature. That

makes the alloy try to recover its initial shape, generating a compression force. This is the force wanted to deliver to the tendon systems.

The parameters that regulate the actuation of the SMA spring are the temperature and the deformation. They are required to control the actuation. The first step to continue working with the spring is to characterize its actuation parameters. Traditionally, the actuation could be modeled by knowing its composition. However, various SMA providers generate a deviation in their characteristics. Therefore, identifying the alloy is crucial to evaluate the actuation.

The identification starts by evaluating the force the actuators can develop in terms of temperature and elongation. The actuator is blocked in a desired elongation, and the temperature and force generated are measured. The identification results conclude that a spring of 1.5 mm of wire diameter and 10 mm of spring diameter, with an elongation of 500% at 180 ºC can exert forces up to 100 N. The behavior evaluated during the identification highlights the possibilities of this alloy to be used as actuators for this kind of alloy. The first characteristic that contributes to the actuation is the superelasticity of the alloy. The SMAs can maintain their properties, having 500% of deformation. The second, also related to the first, is the capability to perform longitudinal displacement. This characteristic makes SMA springs a proper actuator for tendon-driven actuation. The last one exposed in this work is the weight of the actuator. The SMAs used in this work can exert up to 100 N with only 8 g of material. This capability is of interest in aerial robotics, in which weight is one of the main limitations.

The next step is to define the method of actuation of the SMAs. Electrical actuation is proposed to reach the temperature that makes the alloy recover the initial shape. The use of a constant electrical current applied to the extremes of the spring makes the spring increase its temperature. Then, a MOSFET is used to control the time of actuation of this current. The MOSFET opens the circuit during the actuation, stopping the warming process of the SMA. To know the alloy's temperature, a PT100 sensor is glued to the surface of the alloy. Then, a processor translates the data to Celsius. By knowing the temperature and the identification performed in Section 3.2, the alloy state is determined.

To transmit the tension to the tendons, a system of actuation capable of increasing and decreasing the force of actuation is needed. This work proposes the use of an antagonist muscle configuration of the actuation. This system is presented in Figure 7.

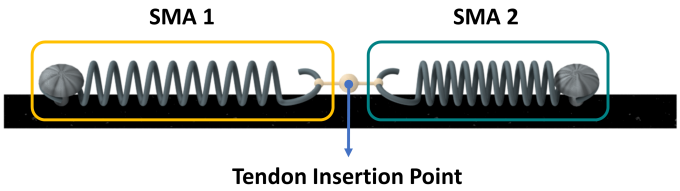

Figure 7. The SMA antagonist muscle configuration. The force generated by *SMA 1* opposite to the *SMA 2*.

In this configuration, the force generated by the *SMA 1* directly opposes the force generated the *SMA 2*. Then, a transmitted tension to the hand tendons results from the two forces. This configuration improves the response time using SMAs, reducing the cooling time. Regarding the actuation of the hand, *SMA 1* pulls the tendons, closing gripper, and *SMA 2* pulls *SMA 1*, reducing the tension applied. Then, the system takes advantage of the differential actuation phases of the alloy, increasing the reaction velocity. The opening motion is managed via the elasticity of the TPU joints recovering the initial shape of the hand. The following section models the actuation to analyze the behavior of the system.

3. Dynamic Modeling

This section presents the actuation model of the manipulation system. It focuses on the inter-relationship between the manipulator and the SMAs. Figure 8 shows the block diagram of the system and the actuators.

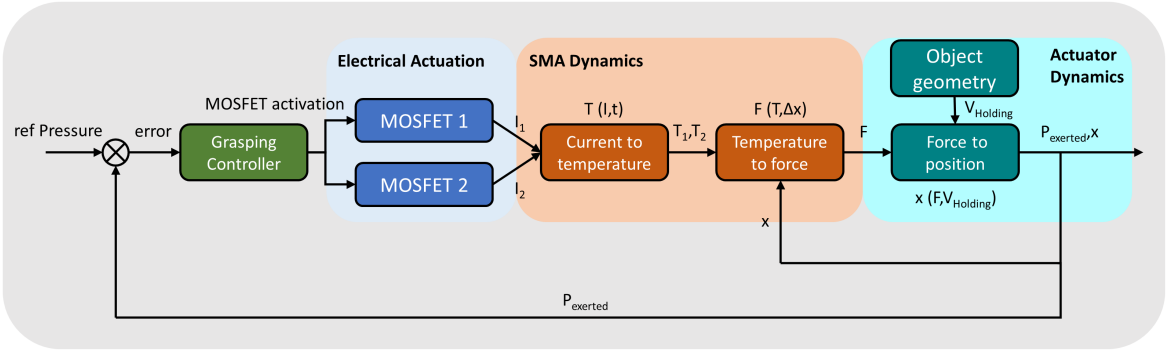

Figure 8. The block diagram of the actuation.

There are four background colors in the figure. The first is gray. This color surrounds the complete figure and all the systems involved in the actuation. The next one is blue. The blue color highlights the electrical actuation of the system. This actuation is performed via two MOSFETs that regulate the inputs of the SMA actuator. The third background color is orange, which involves the model of the SMA in the proposed configuration of this work. It receives the electrical actuation and the spring's position and evaluates its developed force. Finally, the green color shows the model of the manipulator. This model analyzes the absorbed tendon tension to close the hand and deliver pressure to the object.

3.1. Hand Modeling

The developed manipulator follows the concept of a human hand of standard size. To replicate the joints of a human hand, it uses 3D-printed joints that bend against the tension of the allocated tendon inside the hand. This section aims to analyze the motion of the hand in terms of the exerted force by the tendons. Figure 9 presents a schematic of the joints of the hand. Each joint is substituted by a spring with a K constant that has to be identified to model the absorbed force to close the hand.

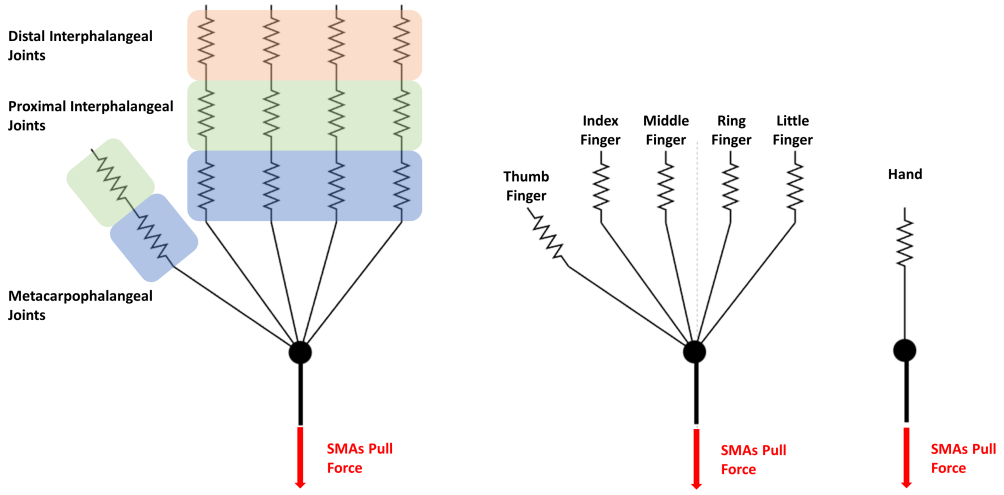

(**a**) (**b**) (**c**)

Figure 9. The hand model identification. The figure shows the identified parameters of the hand to model the motion. (**a**) Joint spring model. (**b**) Finger spring model. (**c**) Hand spring model.

Figure 9a presents the spring that substitutes each of the joints in the manipulator. The spring constant depends on the material and the geometry of the fingers. Like humans, the force needed to close the fingers is low. However, the elongation is limited, increasing the weight of the objects manipulated. These characteristics influence the design of the hand joints. The model aims to evaluate the parameter that regulates closing movement. For that purpose, it models each joint as a spring. Figure 9b from its side combines each

finger's joints and replaces them for equivalent springs. Then, Figure 9c identifies the equivalent spring that models the whole manipulator. The spring that models the entire hand also includes the communication of the force between the different fingers.

Different parameters influence the model of holding. Starting from the joint geometry, the thickness of the joint and the longitude between phalanxes are the main parameters of the bending. However, as the joint is 3D printed using flexible TPUs, the internal parameter of the joint and the printing conditions must be considered to develop an appropriate model. Each joint could be evaluated as a cantilever beam in which a force is applied at a distance from the center, generating a moment to bend the joint. This approach helps to analyze the critical point of bending. However, the actuation system is complex, and other factors, like the friction between the tendons and their ducts, are challenging to consider. Therefore, this paper analyzes the system to extract the equation of motion for the holding phase. The objective is to evaluate the K constant of the joints using a load cell and to evaluate the generated force against the displacement. Then, the relationship between the different constants of the joints and the actuation of the entire hand will be obtained.

The analysis starts with evaluating the spring constant of the fingers. The process for assessing this motion consists of pulling a finger's tendon against the load while measuring the displacement. Ultimately, the process obtains the generated force in terms of the displacements. The equation that models this behavior could be evaluated. Figure 10, left side, shows the graphical results of the different fingers of the hand.

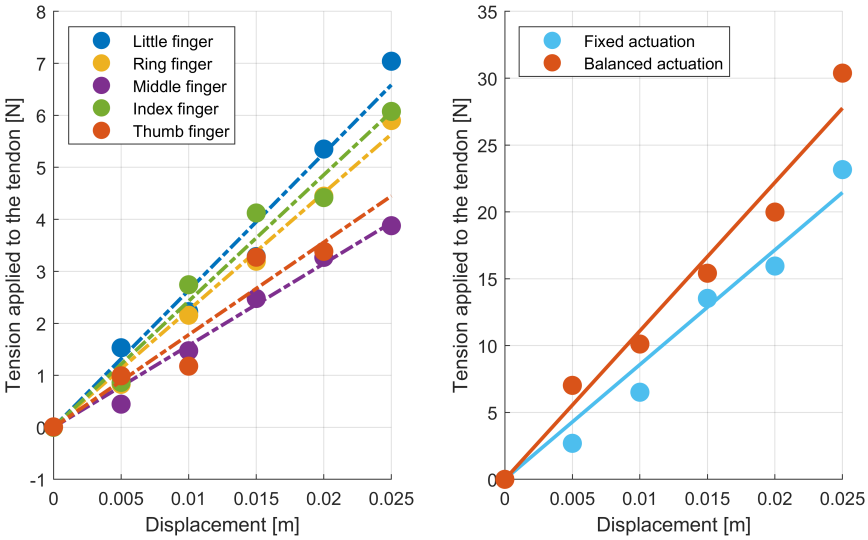

Figure 10. Model of hand performance. **Figure left** side force/displacement of each finger has been measured. **Figure right** side measurement of the force/displacement of the whole hand as a function of the actuation balance.

These results show the needed force to close each finger of the claw separately. Then, a system of balance tendons connects the fingers with the SMA actuation. The force applied to each finger varies depending on the balanced system's configuration. This work contemplates two possibilities. In the first one, all the fingers are simultaneously connected to the closing motion's end. This configuration aims to communicate the same force to all the fingers. The second configuration consists of balancing the force between the different fingers. So, if one of the fingers gets stuck, the rest of the hand continues with the motion, improving the adaptability of the hand to non-homogeneous surfaces. Figure 10, right side, shows the results for both configurations.

The identification results show that the hand model can be approximated as a spring with a linear constant K. These results allow the drive to be modeled with the following equation:

$$F_{\text{hand}}(x_{\text{SMA}}) = K_{\text{hand}} x_{\text{SMA}}, \tag{1}$$

where F_{hand} is the needed force to close the hand depending on the spring displacement x_{SMA}, and K_{hand} is the identified constant that depends on the actuation's balance. The next step to model the actuation is to evaluate the grasping motion of the hand around the objects. The holding volume of the objects characterizes this behavior. Then the displacement that SMAs actuation can perform was analyzed before being stuck with the surface. This displacement and the hand's contact area make it possible to calculate the exerted pressure.

3.2. SMA Actuation Modeling

The first step in modeling the SMA is to define the actuation procedure. This work uses electric currents to vary the temperature of the alloy. So, SMAs are a resistor that transforms electrical energy into thermal energy. However, the electrical behavior of SMAs depends on the alloy and must be modeled. Some authors point out that this equivalent resistance varies with temperature. This work supplies a constant current to the actuator measuring the voltage generated to analyze the behavior of the alloy used. Then, by changing the current supply, the alloy reaches different temperatures, allowing it to analyze the behavior with temperature. Figure 11 shows the results of these identification processes.

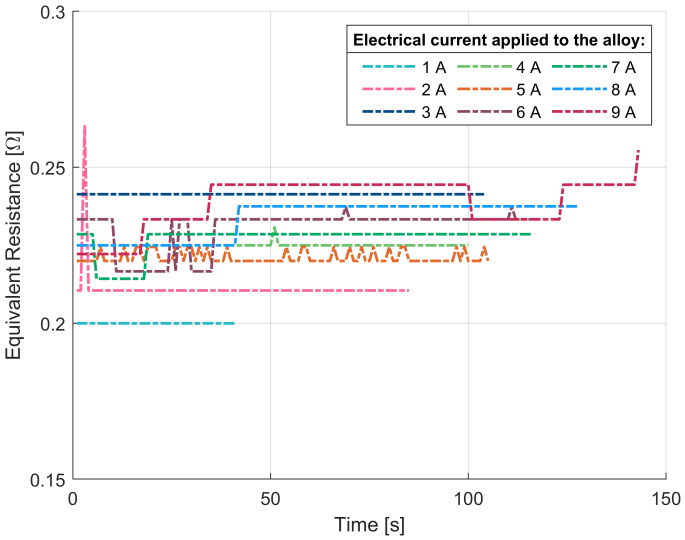

Figure 11. The electrical resistance in terms of the temperature and applied current to the system.

Figure 11 shows that the equivalent resistance of the SMA is almost stable with the temperature. Some disturbances were found due to the measurement instruments; however, the resistance value could be assumed as the average value. In this case, the instant power consumption of the SMA is modeled as follows:

$$P_{\text{consumed}}(I) = I^2 R_{\text{SMA}}, \tag{2}$$

where I is the electrical current consumed by the alloy, and R_{SMA} is the equivalent resistor of the spring. To evaluate the transferred power to the environment, it is known that the maximum temperature with a determined and stable electrical supply defines the power to the system. The delivered power to the environment is the same. Table 1 presents these parameters, measured from the alloy employed in this work.

Table 1. The maximum achieved temperature regarding the current supplied to the alloy.

Electrical Current [A]	Instant Consumed Power [W]	Time [s]	Temperature [K]	Consumed Energy [J]
1	0.2	21	296.9	4.2
2	0.76	72	303	54.8
3	2.03	93	313.9	188.8
4	3.6	91	328.4	327.8
5	5.5	89	341.7	487.8
6	8.3	103	363.5	853.1
7	11.2	112	380.5	1245.3
8	14.9	117	401.1	1745.2
9	19.33	140	437.8	2704.6

In Table 1, **Electrical Current** is the current supplied to the spring, **Instant Consumed Power** is the consumed one during the actuation, **Temperature** is the maximum reached temperature during the actuation, **Time** is the time to reach this temperature, and **Consumed Energy** is the total energy provided to reach this temperature. With temperature and power consumption, the following equation is assumed:

$$P_{\text{consumed}}(I, T_{\text{max}}) = P_{\text{transferred}}(T_{\text{max}}), \tag{3}$$

where $P_{\text{consumed}}(I, T_{\text{max}})$ is the consumed power by the system at the maximum temperature with a specified power supply, and $P_{\text{transferred}}(T_{\text{max}})$ is the transferred power to the environment. Then, the transference of the system has been modeled as a resistor exchanging energy with the environment. The following formulation models the behavior:

$$P_{\text{transferred}} = hA(T - T_{\text{environment}}), \tag{4}$$

where h is the heat transfer coefficient, and A is the area in contact with the air.

The coefficient hA is obtained from the presented data in the previous table. Finally, the energetic behavior of the spring is modeled. The model can analyze the energetic exchanges of the alloy in terms of temperature. This makes it possible to have the temperature of the spring, knowing the supplied energy. The total energy stored in the spring can be calculated as follows:

$$E_{\text{consumed}}(T, t, I) = E_{\text{usefull}} + E_{\text{transferred}}, \tag{5}$$

where $E_{\text{consummed}}$ is the total energy consumed by the alloy in a time t to reach a temperature T using an electrical current of I. E_{useful} is the energy stored in the spring to reach the temperature, and $E_{\text{transferred}}$ is the energy that the spring delivers to the environment in the warming process. Then, these terms are calculated by integrating the instant powers as follows:

$$E_{\text{consumed}}(I, t, T) = \int_{t(T_0)}^{t(T)} [P_{\text{consumed}}] \mathrm{d}t, \tag{6}$$

$$E_{\text{transferred}}(t, T) = \int_{t(T_0)}^{t(T)} [P_{\text{transferred}}] \mathrm{d}t, \tag{7}$$

where $t(T)$ is the time invested to reach the temperature T and $t(T_0)$ is the initial temperature in time and temperature. Finally, the energetic behavior of the spring is known. The first step is to describe the SMAs' actuation performances in the system. This work

uses an antagonist muscle method in which one SMA spring applies tension to the tendon, and the other opposes this force, as presented in Figure 7.

The actuation method is essential for analyzing the model. In this case, one spring pulls the other during the entire actuation process. As detailed previously, SMAs have two possible internal structures depending on the temperature, martensite, and austenite. In this case, it is considered that the model starts from the deformation performed at 100% of the martensite phase. Then, the parameters to be considered for modeling the SMA dynamics are the temperature and the elongation of the spring. The system is modeled as a spring with an elongation constant in terms of temperature and extension. The following equation defines the dynamic behavior of the SMA spring:

$$F_{\text{SMA}}(T, x) = F_{\text{martensite}} + K\Delta T\Delta x, \tag{8}$$

where F_{SMA} is the generated force by the SMA on a determined temperature T and position x. $F_{\text{martensite}}$ is the needed force to perform a plastic deformation at 100% of the martensite phase. $F_{\text{martensite}}$ was identified from the alloy by performing a constant deformation on the spring, measuring the delivered force with a load cell. Then, several tests were conducted to analyze the value of K, varying the temperature with different elongations. The interrelationship between the energetic and dynamic models determines the behavior of the SMA actuation. The energetic model provides the temperature of the spring in terms of the supplied power. The dynamic model receives as inputs the elongation of the spring from the model of the hand and the temperature from the energetic model. Then, the model processes the data and delivers the force generated by the SMA antagonist configuration to the hand model.

3.3. Modeling Results

Figure 12 shows the results of the developed model. The input to the model is the pressure wanted to be applied to the grasped object. The activation of the SMAs muscles is then controlled using a hysteresis controller with a band of 100 Pa. In this case, the power supplied to the actuation is 3.7 V, the nominal value of a LiPo battery cell. The model of the SMAs calculates the tension exerted on the tendons as a function of the current received and the time of activation. The grasping model translates the force into a displacement on the actuator and pressure around the object. The approach considers the gripping volume of the object to calculate the pressure and displacement. Figure 8 shows the relationships between the models.

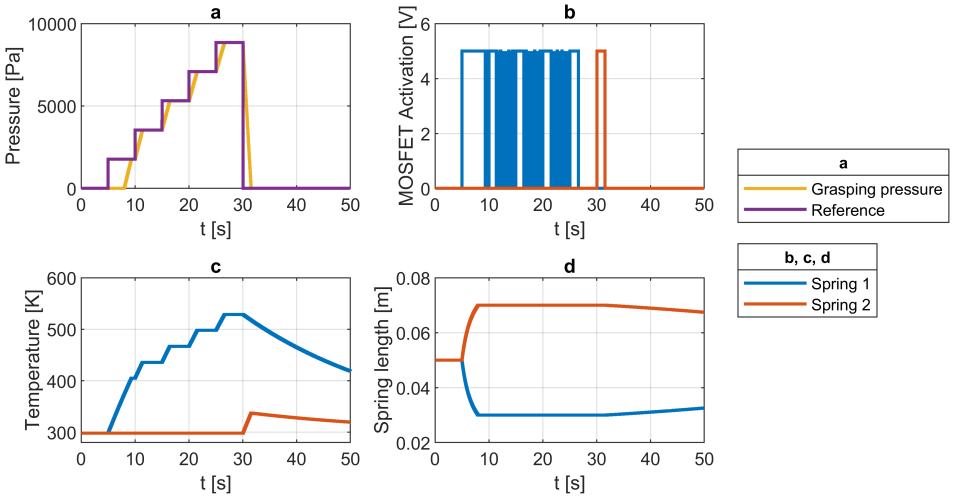

Figure 12. Modeling results of the following: (**a**) pressure reference and actuation, (**b**) spring activation, (**c**) springs temperatures, and (**d**) lengths of the springs.

Figure 12a shows the reference in purple and the pressure exerted on the object in yellow. The controller in this theoretical validation is a hysteresis controller that receives feedback from the grasping model. The results show that the actuation can follow the reference. Figure 12b–d show the parameters of actuation of the SMA, the time of activation in b, the spring temperature in c, and the spring length in d. The input to the model is an incremental step signal in grasping pressure.

The hand gripper is wholly opened at the beginning of the actuation. Then, the controller increases the temperature of the $Spring1$ to reach the desired pressure. The tension applied to the tendons increases with the temperature and elongation of $Spring1$. The actuation follows the pressure increment feeds. The length of the springs in Figure 12d is blocked while the hand is in contact with the object's surface, as shown in the chart, between 8 and 30 s. $Spring2$ is the antagonist, which manages to decrease the tension applied to the tendons. $Spring2$ is activated between seconds 30 and 33. The activation of this muscle reduces the pressure exerted to 0 Pa. $Spring2$ should continue being actuated to reach the initial elongation of the springs opening the hand completely. However, in the case of delivering, the object falls due to the absence of grasping forces, making it unnecessary to extend the hand completely. The theoretical model demonstrates that the solution is achievable. Furthermore, the results are coherent with the dynamics and the behavior observed from the SMAs. This model aims to estimate the exerted pressure on the grasped objects in terms of the temperature of the SMA springs. Then, by using it and having the object's volume, the actuation can be controlled, increasing the safety of manipulating fragile objects.

4. Experimental Validation

The experimental validation of the manipulator aims to analyze its behavior in holding different objects, testing its adaptability, and using the prototype in aerial applications. In that sense, the section is divided into grasping and on-board experiments.

4.1. Grasping Experiments

In this section, the capabilities of the hand to grasp different objects are analyzed. The aim is to evaluate the adaptability of the manipulator, testing it with varying geometries and weights. Figure 13 summarizes the grasping experiment focusing on daily-life objects and different tools and devices used on the powerline inspection and maintenance.

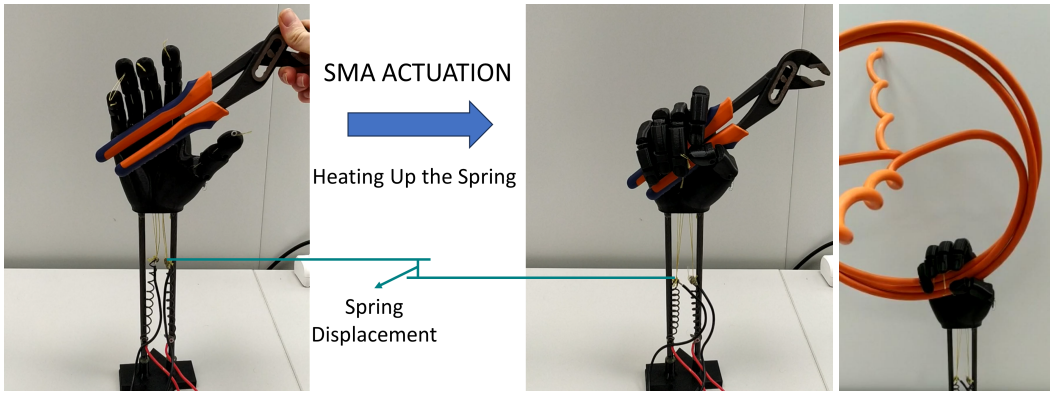

Figure 13. *Cont.*

Figure 13. Grasping experiments. (**a**) Slip joint plier. (**b**) Powerline bird diverter. (**c**) Diagonal plier. (**d**) Thermal bottle. (**e**) Soft drink can. (**f**) Adjustable wrench. (**g**) Diagonal plier horizontal grasping. (**h**) Diagonal plier one handle grasping. (**i**) Diagonal plier grasping test.

The developed device aims to work together with workers on the powerline. With that purpose, this section tests the ability to hold tools commonly used in the powerline in Figure 13a–c,f. The system proves that it can perfectly manage the characteristics of this kind of object and adapts to the shape of the items. However, cooperation in this kind of work imposes some necessities for the workers. The ability of the system to transport some drinks and other essential hydration devices. The variety of the sample is enough to evaluate the hand's behavior. Table 2 shows the main characteristics of the objects that influence the manipulation.

Table 2. The parameters of the grasped objects using the manipulator.

Object	Weight [g]	Grasping Volume [cm^3]
Slip joint plier	453	91.2
Power line bird diverter	630	31.6
Diagonal plier	227.1	72.35
Thermal bottle	300	421.2
Soft drink can	15	292.5
Adjustable wrench	413	53.75
Power line phase separator	1026	53.72
Stockbridge damper	2232	205.2

To show the variety of the samples, Figure 14 displays the weight of the grasped object and the volume.

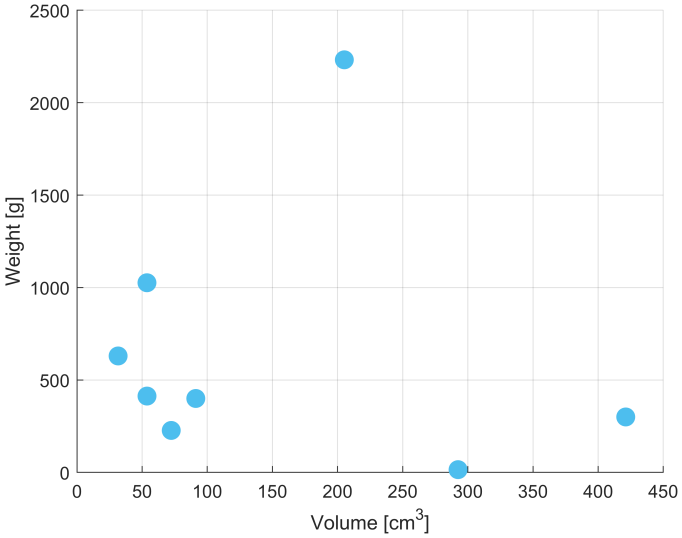

Figure 14. Characteristics of the grasped objects.

Knowing the grasped object's characteristics, the manipulator's performance is evaluated. The manipulator of 225 g (including electronics) proves that it can manage a manipulation of up to 2.5 kg of payload with a volume of 205 cm^3. The grasping capacity tested from 31 to 421 cm^3 proves the manipulator's adaptability. Concerning the SMA actuation, Figure 13a shows the generated displacement to hold the slip joint plier. This displacement decreases with the hold volume. This caused an increase in the exerted force via the SMA in the object with a larger volume at the same temperature as the alloy. However, the temperature is controlled to guarantee the safety during the operation. The next step is to analyze the torque that the manipulator can generate.

The experiments shown in Figure 13g–i evaluate the capability of the hand to maintain grasping in different orientations and object positions. Figure 13g proves that the hand can maintain the object in the horizontal direction. Figure 13h,i analyze a scenario where the plier is not perfectly allocated inside the hand. Figure 13h graphically realized the grasping volumes the gripper can manage. The volume inside the gripper in this figure is less than half of those in Figure 13c,g, maintaining the same weight. Figure 13g is particularly interesting in analyzing the soft capabilities of the actuator. The figure shows the performed deformation on the fingers during the grasping. The performed deformation during this grasping ensures the behavior of the actuator while manipulating fragile objects. Ultimately, the experiments presented in these figures demonstrate the capability to maintain the object's holding under possible flight uncertainties. The AHH is prepared to work on powerlines. So, it is interesting to evaluate the generated grip in different sizes of cylindrical objects. The capabilities added by silicone are essential in torque generation. In that way, the manipulator includes the skin and palm structure for these experiments. Figure 15 shows the results of these experiments.

The figure shows the generated torque via the actuator in terms of the tendon tension with cylindrical polished surfaces. The experiment focused on two objects 45 mm and 58 mm in diameter. The results show that the generated torque is proportional to the tension on the tendons in both cases. The generated grip in the smaller object is bigger. This behavior is due to the resultant forces generated by the fingers where the fingers wrap it completely. This reduces the stresses caused by the object opening the manipulator. In the second case, the hand can exert less torque; however, the results in both cases are good, demonstrating the hand can manipulate these geometries.

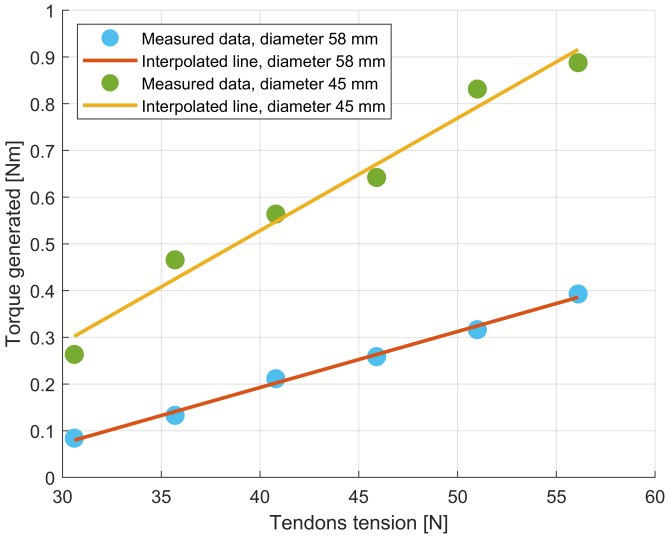

Figure 15. The torque experiments. The figure shows the generated torque by the manipulator for different cylindrical objects.

4.2. On-Flight Experiments

This section analyzes the actuator's capabilities during flight, installed in the aerial platform. In aerial robotics, it is crucial to maintain the behavior of the developed devices while flying. The manipulator design combines novel material with lightweight actuation methods to make the flight of the aerial robot in the best possible condition. Figure 16 represents the systems developed to integrate the manipulator into the aerial platform.

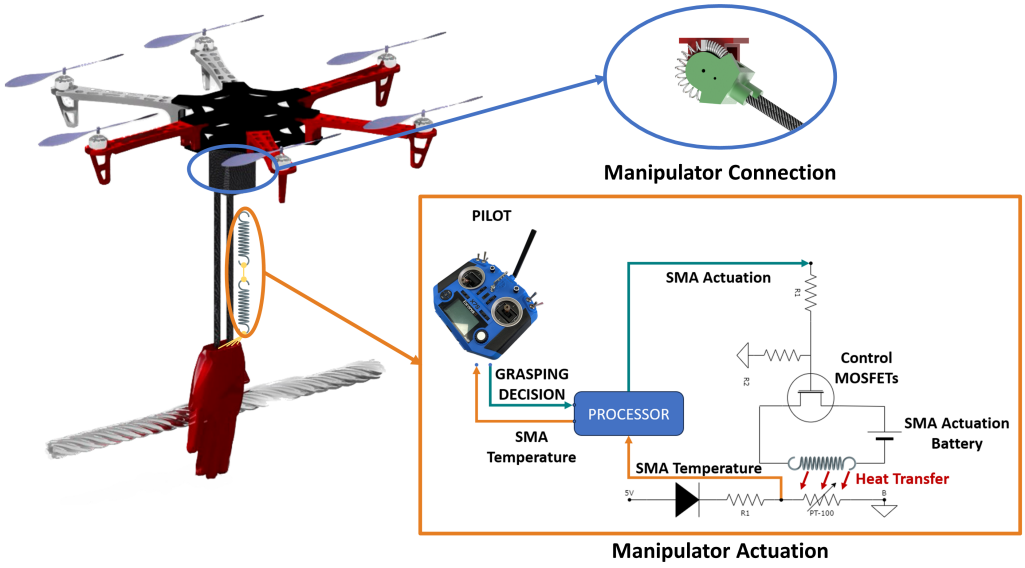

Figure 16. The onboard setup. The figure represents the onboard setup used during the on-flight experimentation. It includes the electronics to actuate the hand, the system to integrate the manipulator in different aerial platforms, and a diagram of the SMA actuation.

Figure 16 shows the mechanical, electronic, and control integration of the gripper into the aerial platform. Starting from the mechanical point of view, the manipulator is connected to an underactuated joint using two carbon fiber bars of ten millimeters in diameter and 50 cm in length. The space between the end-effector and the aerial platforms increases the distance between the manipulation volume and the propellers. This characteristic improves safety during the operation. The bars are also used to place the SMA actuation system. The length generated makes it possible to improve the accuracy

of the SMA actuation. The underactuated joint, shown in the figure surrounded by blue lines, is a rotational joint damped via a spring system. It makes the system compliant with the motion of the end effector and always repositions the manipulation system's load in the center of mass of the aerial platform, reducing the disturbances generated by the manipulator during flight. This system makes it possible to land and take off with the usual landing systems of commercial drones. The manipulator only requires six screws to install the system at the bottom of the aerial platform. Combined with the underactuated joint, it makes the manipulator suitable for different UAVs. The system was tested in two types of medium size commercial UAVs during the experimentation: the hexacopter DJI F550 (Figure 17b–f) and the quadcopter S500 (Figure 17a). The requirement for the platforms to use this manipulation system is to have a remaining payload of around 300 g and a distance between the platform's bottom frame and the floor of 15 cm.

The second part of the figure, surrounded by orange lines, focuses on the electronic integration and the control setup during the flight experiments. During the flight experimentation, the pilot of the aerial platform controls the gripper actuation. The model developed in the previous section is used to have an approximation of the force that the actuator is exerting. It helps the pilot to make the grasping decision. However, it is not crucial due to the soft characteristics of the actuator. To provide the information needed by the model, a PT100 temperature sensor was installed on the SMA with a tension divider to measure the temperature of the SMA. This information and the initial condition of the SMA actuation are provided to an Arduino nano that measures this signal and transmits it using the serial port to the onboard computer. Then, the onboard computer sends the information to the ground station via WIFI. Therefore, the pilot has all the information to proceed with the grasping.

The pilot sends the grasping signal via radio using the RC controller to open or close the actuation system. The RC receiver receives this signal and transmits it to the processor onboard. The processor onboard manages this signal and opens or closes the circuit using the MOSFET, as shown in Figure 16. The system's actuation has independent batteries to avoid possible interferences in the flight system. The batteries are two small LIPO cells of 500 mAh used in a parallel configuration with a discharge rate of 95C. These batteries weigh 10 g each, minimizing the system's total weight.

Figure 17 summarizes the on-flight experiments. They focus on the delivery of various objects of different sizes. Furthermore, the capabilities provided by the underactuated joint during the flight have been tested in Figure 17a taking a face shield from a dummy's head. The system could absorb the flight disturbances, making it possible to take the object.

One objective of this work is the co-operation of the robot with humans. The actuator uses a soft structure and skin to reduce operational risks. Figure 17a evaluates this capability by approaching the actuator active to a dummy representing an operator. The manipulator shows that it can crash, touch, and take the face shield from the head of the symbolized worker without performing any damage. This experimentation continues with object delivery to evaluate the device's capability to hold while flying and deliver it in specific locations. These tests demonstrated the SMA's ability to control the actuation of the manipulator. The developed device keeps holding the object, absorbing the inertia of the motion generated by the multi-rotor flight. The conducted tests also demonstrated the behavior of the developed onboard electronics. This setup has to manage high electrical power to warm the alloy with reduced weight. It makes it necessary to reduce the weight of specific components like dissipators. However, the system demonstrated that it could manage this overload safely. Figure 17b–f presented the load that the onboard system could afford. Comparing these results with the weight of the system, they are exceptional. They preserve the capabilities shown in the testbench experiments. The soft actuation and contact combined with a printed structure show unusual behavior in manipulating rigid objects up to delicate touches.

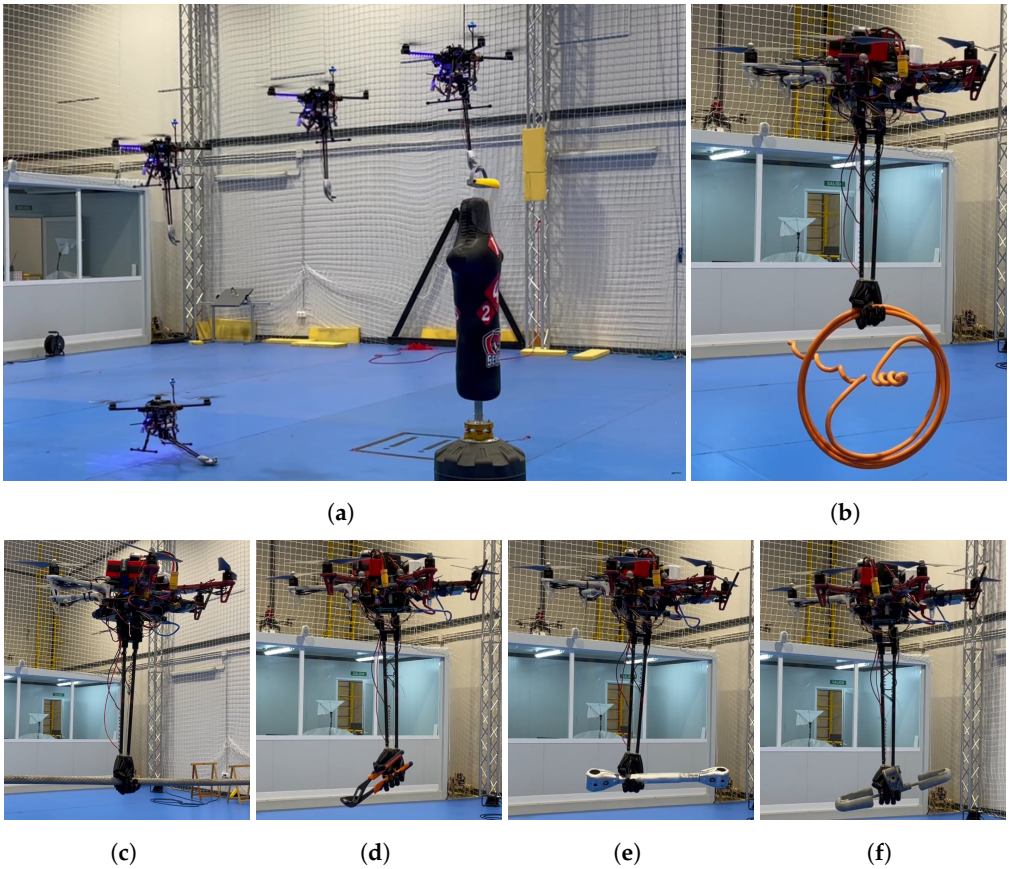

(**a**) (**b**)

(**c**) (**d**) (**e**) (**f**)

Figure 17. Flight experiments. (**a**) Face shield. (**b**) Power line bird diverter. (**c**) Powerline. (**d**) Slip joint plier. (**e**) Power line phase separator. (**f**) Stockbridge damper.

The developed hand is classified inside the family of soft robotics grippers as a tendon-driven SMA actuated gripper, following the developed classification by the authors in [37]. This actuator combines two kinds of soft actuation: tendon-driven and SMAs. The main difference between this gripper and others is the following high relationship: *weight of the objects manipulated/weight of the manipulation system*. The gripper can manage objects up to 13 times more weight than the total weight of the actuation system. This characteristic makes this device proper for its use in aerial robotics. The adaptability of the system shown during the experimental validation surpasses the examples found in the literature for a tendon-driven gripper. Ultimately, using these grippers in aerial robotics is rarely reported in the literature.

Table 3 presents an objective comparison between the different grippers used for aerial robotics. The table focuses on the main skills of a cooperative manipulator for aerial robotics. This study is limited to the data provided by the authors of the compared grippers. The last row of the table presents the data from our manipulator, highlighted in bold text.

Table 3 comprehensively compares different grippers used in aerial robots. The first analyzed parameter is the weight of the system. UAVs have a limited payload capacity; weight reduction will reduce energy consumption and improve maneuverability. In an extreme case and improper design, the weight can prevent the platform from take off. The next parameter is the load that the gripper can manipulate/hold. The best condition for the aerial systems is to improve the weight/mass ratio. Table 3 shows this parameter in the third column. The developed actuator, highlighted in bold text, shows the best ratio compared to relevant scientific reports. The closer one is a magnetic gripper only applicable for grasping ferromagnetic materials.

Table 3. Aerial robotics grippers comparison.

Gripper	System Weight [g]	Maximun load [kg]	Load/Weight	Actuation Method	Actuators	Adaptability	Soft Contact
Four finger gripper [38]	-	1	-	Tendon driven	Servos	Low (Cylindrical shapes)	No
Underactuated gripping foot [39]	478	-	-	Tendon driven	Passive	Low (Cylindrical shapes)	Yes
Bird inspired claws [40]	250	0.1	0.4	Tendon driven	Springs and servos	Medium (Soft objects)	No
Robotic arm manipulator [41]	900	0.45	0.5	Mechanical	Servos	Low (Plain surfaces)	No
Compliant bistable gripper [42]	9	0.027	3	Bistable system	Passive	Not applicable	Yes
Magnetic gripper [43]	295	2.6	8.81	Magnetic	Magnets and Servos	Not applicable	No
Dual symmetric manipulator [44]	330	0.4	1.21	Mechanical	Servos	Low (Plain surfaces)	No
SMA bird inspired claws [8]	180	0.25	1.4	Tendon driven	SMAs	Medium (Soft objects)	Yes
Anthropomorphic hand	**225**	**3**	**13.33**	**Tendon driven**	**SMAs**	**High (Multiple geometries)**	**Yes**

In the table, the system weight includes the links of the gripper that attaches the system to the aerial robot, the actuators, and control electronics. The maximum load is the maximum one that the manipulator can manage. The actuation method describes the way to develop the force on the gripper actuation. The actuators are the system in charge of generating the force. Adaptability measures the way that the gripper is adapted to multiple geometries. Soft contact analyzes the capabilities of the gripper to provide smooth and adaptable contact

The next column of Table 3 shows the actuation methods usually used in aerial robotics. Tendon-driven actuation is one of the most common methods; however, it used to be combined with other actuation methods like passive systems or servomotors. The SMA-developed actuation in this work surpasses the capabilities of traditional servomotors in terms of weight. The adaptability of the gripper for grasping different objects with size and shape changes is impressive and difficult to find in other aerial robotics grippers. Finally, the last column of Table 3 focuses on the soft capabilities of the different grippers. Human cooperation is one of the major concerns of aerial robotics. The soft adaptability and structure of the hand made it possible to improve the cooperation skills of existing aerial robot solutions. The comparison results highlight the contributions of the developed hand to the current state of the art of aerial robots.

5. Conclusions

This paper investigated the application of aerial manipulation using a human-inspired SMA-actuated gripper for object delivery to human workers, manipulation, carrying, and dropping items using an unmanned flying platform. The application of aerial platforms for device delivery is getting more frequent in the industry, especially for dangerous work, i.e., delivering a device to a human worker at a high altitude or a hard-to-reach place. In order to facilitate the collaboration between the aerial robot and the human worker, soft grippers and human-inspired designs are preferable. This work presented a tendon-driven SMA-actuated design that manipulates objects of different shapes and sizes. An analysis of the geometry of the objects has been conducted and showed successful manipulation for a series of items. Due to the SMA actuators' lightweight characteristics, the drone's payload was increased and dedicated to object transportation. The control of the temperature, which

triggers the SMA material, is a challenge that was addressed. The human-inspired design increased the dexterity of the system in the context of grasping.

Author Contributions: Conceptualization, V.P.-S., F.J.G.-R. and B.A.; methodology, V.P.-S. and F.J.G.-R.; software, V.P.-S. and F.J.G.-R.; validation, V.P.-S. and F.J.G.-R.; formal analysis, V.P.-S. and F.J.G.-R.; investigation, V.P.-S. and F.J.G.-R.; resources, V.P.-S. and F.J.G.-R.; data curation, V.P.-S. and F.J.G.-R.; writing—original draft preparation, V.P.-S., F.J.G.-R. and S.R.N.; writing—review and editing, V.P.-S., F.J.G.-R. and S.R.N.; visualization, V.P.-S., F.J.G.-R. and S.R.N.; supervision, S.R.N. and B.A.; project administration, A.O.; funding acquisition, A.O. All authors have read and agreed to the published version of the manuscript.

Funding: This work was supported by the GRIFFIN Advanced Grant of the European Research Council, Action 788247, and the H2020 AERIAL-CORE project under Grant 871479.

Data Availability Statement: Not applicable.

Acknowledgments: The authors thank the GRVC Robotics Lab and Alejandro García Segura and Alberto Trigo Romero for supporting this work.

Conflicts of Interest: The authors declare no conflict of interest.

References

1. Ilami, M.; Bagheri, H.; Ahmed, R.; Skowronek, E.O.; Marvi, H. Materials, Actuators, and Sensors for Soft Bioinspired Robots. *Adv. Mater.* **2021**, *33*, 2003139. [CrossRef] [PubMed]
2. Liu, J.; Zhang, D.; Wu, C.; Tang, H.; Tian, C. A multi-finger robot system for adaptive landing gear and aerial manipulation. *Robot. Auton. Syst.* **2021**, *146*, 103878. [CrossRef]
3. Zhao, Q.; Zhang, G.; Jafarnejadsani, H.; Wang, L. A modular continuum manipulator for aerial manipulation and perching. In Proceedings of the International Design Engineering Technical Conferences and Computers and Information in Engineering Conference, St. Louis, MO, USA, 14–17 August 2022; American Society of Mechanical Engineers: New York City, NY, USA, 2022; Volume 86281, p. V007T07A014.
4. Rodriguez-Castaño, A.; Nekoo, S.R.; Romero, H.; Salmoral, R.; Acosta, J.Á.; Ollero, A. Installation of clip-type bird flight diverters on high-voltage power lines with aerial manipulation robot: Prototype and testbed experimentation. *Appl. Sci.* **2021**, *11*, 7427. [CrossRef]
5. Cacace, J.; Giampetraglia, L.; Ruggiero, F.; Lippiello, V. A Novel Gripper Prototype for Helical Bird Diverter Manipulation. *Drones* **2023**, *7*, 60. [CrossRef]
6. Miková, L.; Medvecká-Beňová, S.; Kelemen, M.; Trebuňa, F.; Virgala, I. Application of shape memory alloy (SMA) as actuator. *Metalurgija* **2015**, *54*, 169–172.
7. Nespoli, A.; Besseghini, S.; Pittaccio, S.; Villa, E.; Viscuso, S. The high potential of shape memory alloys in developing miniature mechanical devices: A review on shape memory alloy mini-actuators. *Sens. Actuators A Phys.* **2010**, *158*, 149–160. [CrossRef]
8. Gomez-Tamm, A.E.; Perez-Sanchez, V.; Arrue, B.C.; Ollero, A. SMA Actuated Low-Weight Bio-Inspired Claws for Grasping and Perching Using Flapping Wing Aerial Systems. In Proceedings of the 2020 IEEE/RSJ International Conference on Intelligent Robots and Systems (IROS), Las Vegas, NV, USA, 24 October 2020–24 January 2021; pp. 8807–8814.
9. Ding, Q.; Chen, J.; Yan, W.; Yan, K.; Kyme, A.; Cheng, S.S. A High-Performance Modular SMA Actuator With Fast Heating and Active Cooling for Medical Robotics. *IEEE/ASME Trans. Mechatronics* **2022**, *27*, 5902–5913. [CrossRef]
10. Niu, D.; Li, D.; Chen, J.; Zhang, M.; Lei, B.; Jiang, W.; Chen, J.; Liu, H. SMA-based soft actuators with electrically responsive and photoresponsive deformations applied in soft robots. *Sens. Actuators A Phys.* **2022**, *341*, 113516. [CrossRef]
11. Yang, S.Y.; Kim, K.; Seo, S.; Shin, D.; Park, J.H.; Gong, Y.J.; Choi, H.R. Hybrid antagonistic system with coiled shape memory alloy and twisted and coiled polymer actuator for lightweight robotic arm. *IEEE Robot. Autom. Lett.* **2022**, *7*, 4496–4503. [CrossRef]
12. Jeong, J.; Hyeon, K.; Jang, S.Y.; Chung, C.; Hussain, S.; Ahn, S.Y.; Bok, S.K.; Kyung, K.U. Soft wearable robot with shape memory alloy (SMA)-based artificial muscle for assisting with elbow flexion and forearm supination/pronation. *IEEE Robot. Autom. Lett.* **2022**, *7*, 6028–6035. [CrossRef]
13. Dharmdas, A.; Patil, A.Y.; Baig, A.; Hosmani, O.Z.; Mathad, S.N.; Patil, M.B.; Kumar, R.; Kottursheettar, B.B.; Fattah, I.M.R. An Experimental and Simulation Study of the Active Camber Morphing Concept on Airfoils Using Bio-Inspired Structures. *Biomimetics* **2023**, *8*, 251. [CrossRef] [PubMed]
14. Abbasi, S.; Mahmood, A.; Khaliq, A.; Imran, M. Reduced order modeling and simulation of a bio-inspired gust mitigating flapping wing UAV. *Int. J. Intell. Robot. Appl.* **2022**, *6*, 587–601. [CrossRef]
15. Jini Raj, R.; Bruce Ralphin Rose, J.; Vasudevan, A. Analysis of Bio-inspired Fishbone Based Corrugated Rib for Adaptive Camber Morphing. *J. Bionic Eng.* **2023**, *20*, 1083–1102. [CrossRef]
16. Perez-Sanchez, V.; Gomez-Tamm, A.E.; Savastano, E.; Arrue, B.C.; Ollero, A. Bio-Inspired Morphing Tail for Flapping-Wings Aerial Robots Using Macro Fiber Composites. *Appl. Sci.* **2021**, *11*, 2390. [CrossRef]

17. Harvey, C.; de Croon, G.; Taylor, G.K.; Bomphrey, R.J. Lessons from natural flight for aviation: Then, now and tomorrow. *J. Exp. Biol.* **2023**, *226*, jeb245409. [CrossRef]
18. Zhu, Z.; Zhao, J.; He, Y.; Guo, S.; Chen, S.; Ji, B. Aerodynamic analysis of insect-like flapping wings in fan-sweep and parallel motions with the slit effect. *Biomim. Intell. Robot.* **2022**, *2*, 100046. [CrossRef]
19. Nekoo, S.R.; Acosta, J.; Ollero, A. Combination of terminal sliding mode and finite-time state-dependent Riccati equation: Flapping-wing flying robot control. *Proc. Inst. Mech. Eng. Part I J. Syst. Control Eng.* **2023**, *237*, 870–887. [CrossRef]
20. Azargoon, Y.; Djavareshkian, M.H. Unsteady aerodynamics of flapping bionic eagle wings in forward flight: An experimental and numerical study. *Proc. Inst. Mech. Eng. Part C J. Mech. Eng. Sci.* **2023**, *237*, 2090–2107. [CrossRef]
21. Li, D.; Zhao, S.; Da Ronch, A.; Xiang, J.; Drofelnik, J.; Li, Y.; Zhang, L.; Wu, Y.; Kintscher, M.; Monner, H.P.; et al. A review of modelling and analysis of morphing wings. *Prog. Aerosp. Sci.* **2018**, *100*, 46–62. [CrossRef]
22. Han, J.H.; Lee, J.S.; Kim, D.K. Bio-inspired flapping UAV design: A university perspective. In Proceedings of the Health Monitoring of Structural and Biological Systems 2009, SPIE, San Diego, CA, USA, 8–12 March 2009; Volume 7295, pp. 466–477.
23. Mannam, N.P.; Duba, P.K.; Sharma, D. Future of Planetary Exploration: Bioinspired Drones for Low Density Martian Atmosphere. In Proceedings of the AIAA SCITECH 2023 Forum, Orlando, FL, USA, 8–12 January 2023; p. 1421.
24. Afakh, M.L.; Sato, H.; Takesue, N. A Study towards a Flapping Robot Maintaining Attitude during Gliding. *Int. J. Adv. Sci. Eng. Inf. Technol.* **2023**, *13*, 681–687. [CrossRef]
25. Nekoo, S.R.; Feliu-Talegon, D.; Acosta, J.A.; Ollero, A. A 79.7 g Manipulator Prototype for E-Flap Robot: A Plucking-Leaf Application. *IEEE Access* **2022**, *10*, 65300–65308. [CrossRef]
26. de Croon, G. Flapping wing drones show off their skills. *Sci. Robot.* **2020**, *5*, eabd0233. [CrossRef] [PubMed]
27. Bao, C.; Kim, T.H.; Kalhori, A.H.; Kim, W.S. A 3D-printed neuromorphic humanoid hand for grasping unknown objects. *Iscience* **2022**, *25*, 104119. [CrossRef]
28. De Pascali, C.; Naselli, G.A.; Palagi, S.; Scharff, R.B.; Mazzolai, B. 3D-printed biomimetic artificial muscles using soft actuators that contract and elongate. *Sci. Robot.* **2022**, *7*, eabn4155. [CrossRef] [PubMed]
29. Wang, C.; Liu, Y.; Qu, X.; Shi, B.; Zheng, Q.; Lin, X.; Chao, S.; Wang, C.; Zhou, J.; Sun, Y.; et al. Ultra-stretchable and fast self-healing ionic hydrogel in cryogenic environments for artificial nerve fiber. *Adv. Mater.* **2022**, *34*, 2105416. [CrossRef]
30. Zhou, H.; Tawk, C.; Alici, G. A 3D printed soft robotic hand with embedded soft sensors for direct transition between hand gestures and improved grasping quality and diversity. *IEEE Trans. Neural Syst. Rehabil. Eng.* **2022**, *30*, 550–558. [CrossRef]
31. Abd, M.A.; Ingicco, J.; Hutchinson, D.T.; Tognoli, E.; Engeberg, E.D. Multichannel haptic feedback unlocks prosthetic hand dexterity. *Sci. Rep.* **2022**, *12*, 2323. [CrossRef]
32. D'Angelo, S.; Pagano, F.; Ruggiero, F.; Lippiello, V. Development of a Control Framework to Autonomously Install Clip Bird Diverters on High-Voltage Lines. In Proceedings of the 2023 International Conference on Unmanned Aircraft Systems (ICUAS), Warsaw, Poland, 6–9 June 2023; pp. 377–382.
33. De La Zerda, S.; Rosselli, L. Mitigating collision of birds against transmission lines in wetland areas in Columbia by marking the ground wire with bird flight diverters (BFD). In *Environmental Concerns in Rights-of-Way Management*; Elsevier: Amsterdam, The Netherlands, 2002; pp. 395–402.
34. Liang, C.; Rogers, C. Design of shape memory alloy springs with applications in vibration control. *J. Vib. Acoust.* **1993**, *115*, 129–135. [CrossRef]
35. Kim, S.; Hawkes, E.; Choy, K.; Joldaz, M.; Foleyz, J.; Wood, R. Micro artificial muscle fiber using NiTi spring for soft robotics. In Proceedings of the 2009 IEEE/RSJ International Conference on Intelligent Robots and Systems, St. Louis, MO, USA, 10–15 October 2009; pp. 2228–2234.
36. Chauhan, A.; Patel, S.; Vaish, R.; Bowen, C.R. A review and analysis of the elasto-caloric effect for solid-state refrigeration devices: Challenges and opportunities. *MRS Energy Sustain.* **2015**, *2*, E16. [CrossRef]
37. Shintake, J.; Cacucciolo, V.; Floreano, D.; Shea, H. Soft Robotic Grippers. *Adv. Mater.* **2018**, *30*, 1707035. [CrossRef]
38. Pounds, P.E.; Dollar, A. Hovering stability of helicopters with elastic constraints. In Proceedings of the Dynamic Systems and Control Conference, Nara, Japan, 12–15 September 2010; Volume 44182, pp. 781–788.
39. Doyle, C.E.; Bird, J.J.; Isom, T.A.; Kallman, J.C.; Bareiss, D.F.; Dunlop, D.J.; King, R.J.; Abbott, J.J.; Minor, M.A. An Avian-Inspired Passive Mechanism for Quadrotor Perching. *IEEE/ASME Trans. Mechatronics* **2013**, *18*, 506–517. [CrossRef]
40. Roderick, W.R.; Cutkosky, M.R.; Lentink, D. Bird-inspired dynamic grasping and perching in arboreal environments. *Sci. Robot.* **2021**, *6*, eabj7562. [CrossRef] [PubMed]
41. Kim, S.; Choi, S.; Kim, H.J. Aerial manipulation using a quadrotor with a two DOF robotic arm. In Proceedings of the 2013 IEEE/RSJ International Conference on Intelligent Robots and Systems, Tokyo, Japan, 3–7 November 2013; pp. 4990–4995.
42. Zhang, H.; Sun, J.; Zhao, J. Compliant Bistable Gripper for Aerial Perching and Grasping. In Proceedings of the 2019 International Conference on Robotics and Automation (ICRA), Montreal, QC, Canada, 20–24 May 2019; pp. 1248–1253.

43. Fiaz, U.A.; Abdelkader, M.; Shamma, J.S. An Intelligent Gripper Design for Autonomous Aerial Transport with Passive Magnetic Grasping and Dual-Impulsive Release. In Proceedings of the 2018 IEEE/ASME International Conference on Advanced Intelligent Mechatronics (AIM), Auckland, New Zealand, 9–12 July 2018; pp. 1027–1032.
44. Yu, P.; Wang, Z.; Wong, K. Exploring aerial perching and grasping with dual symmetric manipulators and compliant end-effectors. *Int. J. Micro Air Veh.* **2019**, *11*, 1756829319877416. [CrossRef]